Displacement Damage Effects in Pinned Photodiode CMOS Image Sensors

Cedric Virmontois, *Student Member, IEEE*, Vincent Goiffon, *Member, IEEE*, Franck Corbière, Pierre Magnan, *Member, IEEE*, Sylvain Girard, *Senior Member, IEEE*, and Alain Bardoux

***Abstract*—This paper investigates the effects of displacement damage in Pinned Photodiode (PPD) CMOS Image Sensors (CIS) using proton and neutron irradiations. The DDD ranges from 12 TeV/g to 1.2×10^6 TeV/g. Particle fluence up to 5×10^{14} n.cm^{-2} is investigated to observe electro-optic degradation in harsh environments. The dark current is also investigated and it would appear that it is possible to use the dark current spectroscopy in PPD CIS. The dark current random telegraph signal is also observed and characterized using the maximum transition amplitude.**

***Index Terms*—Active pixel sensor (APS), CMOS image sensor (CIS), displacement damage dose (DDD), monolithic active pixel sensor (MAPS), pinned photodiode (PPD).**

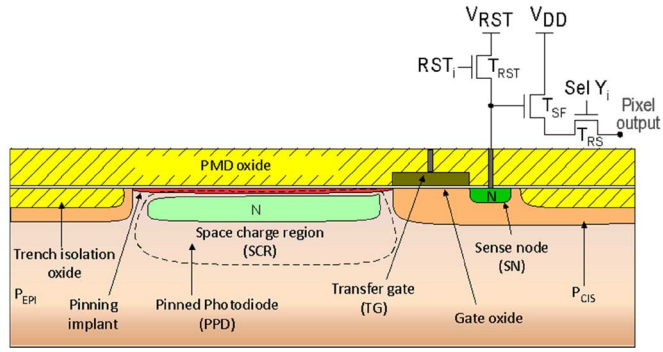

Fig. 1. Cross section of a pixel using the pinned photodiode (4T Pixel CIS). The space charge region appears as a buried bubble.

I. Introduction

PINNED PHOTODIODE (PPD) CMOS image sensors (CIS) [1], also called 4T pixel CIS, are the result of the continuous improvements in image-dedicated CMOS technology. These devices reach very high performance levels, compared to conventional CIS based on 3T pixels, particularly in terms of dark current and noise. It is therefore interesting to study pinned photodiode technology for scientific applications, space missions in particular, especially since the first Earth imaging 3T pixel CIS is already in space. PPD CIS are largely used for commercial applications and is a serious candidate to equip future scientific instruments operated with harsh radiation environments. However, few studies focused on the behavior of this CIS technology under radiation are available. Moreover, as illustrated in Fig. 1, due to its specific architecture using an additional transistor and a charge transfer during operation, 3T CIS device radiation data previously obtained may not directly be applicable to PPD CIS devices. First, the effects of the total ionizing dose (TID) are investigated in PPD CIS [2]–[4]. However, the TID effect in such devices is not yet fully understood. In terms of displacement damage, no dedicated studies on PPD CIS have yet been carried out, (some studies report proton irradiation results [3] but mainly to emphasize TID effects) while more results exist on conventional 3T pixel CIS [5]–[10]. Displacement damage effects are a key issue for solid state imagers exposed to space radiation environments [5] or used in nuclear physics experiments [8]. This work is intended to be a dedicated study on displacement damage effects in PPD CIS devices for possible future use in various radiation environments. Electro-optic and dark current performances are characterized before and after proton and neutron irradiations. Specific devices were irradiated up to a DDD of 1.2×10^6 TeV/g to observe the radiation impact on image quality, the external quantum efficiency and charge-to-volt conversion factor. The dark current and the associated random telegraph signal (DC-RTS) are measured and analyzed for the totality of the DDD range investigated. Since the dark current exhibited by in PPD CIS is of an extremely low level, the dark current spectroscopy (DCS) [9] technique can be applied and is investigated after irradiation.

II. Experimental Details

The imager studied, called IC, has been specially designed for the displacement damage dose analysis. It features 7 μm-pitch 256 $\times$256 pixel arrays with 4T pixel CIS using a pinned photodiodes. This circuit is manufactured using 0.18 μm commercial CIS process. In order to minimize the number of interactions per pixel and the associated number of created defects per interaction, the depleted volume of the photodiode is reduced to just 4 μm ^{3}. Each pixel consists of only four transistors. No additional transistor is used to implement other in-pixel functions like anti-blooming, thus giving the basic in-pixel readout. The array is read in rolling shutter mode with correlated double sampling and the chip output is the analogue signal.

As we can see in Figs. 1 and 2, PPD CIS and 3T pixel CIS are different. 3T refers to three transistors readout, generally composed of a ReSeT transistor, $\mathrm{T_{RST}}$, a Source Follower tran-

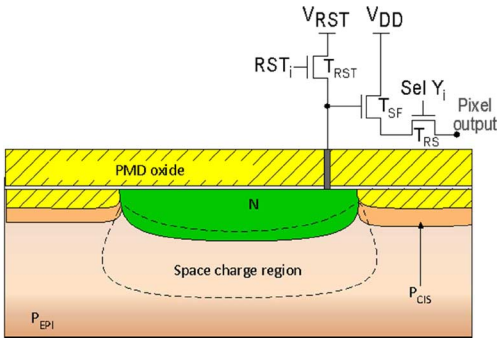

Fig. 2. Cross section of a pixel using a conventional photodiode (3T pixel CIS).

sistor, $\mathrm{T_{SF}}$ and Row Select transistor, $\mathrm{T_{RS}}$. The 4T configuration adds a transfer transistor, whose transfer gate is illustrated in Fig. 1, between the pixel and the previously named three transistors. Another main difference is the photodiode which consists of $\mathrm{P^+/N/P}$ sandwich resulting in a buried photodiode. For 4T pixel CIS, the photo-generated charges are collected inside this potential well during the integration time. The accumulated charges are then transferred through the additional transistor $(\mathrm{T_G})$ to the sense node. Finally, the potential of the sense node, proportional to the integrated charge, is read in the same way as conventional 3T pixels using the three other transistors $(\mathrm{T_{RST}}, \mathrm{T_{SF}}, \mathrm{T_{RS}})$ [11].

A key element of the 4T pixel is the bias on the transfer gate during the integration ($\mathrm{V_{low}}$ TG). As already discussed [4], [12], the $\mathrm{V_{low}}$ TG has an important impact on the pixel dark current. Therefore, we decided to use an optimal $\mathrm{V_{low}}$ TG to accumulate the transfer gate during integration and reduce the dark current. If the transfer gate is not accumulated during integration (for example with 0 V bias) the space charge region of the photodiode is extended under the $\mathrm{T_G}$ and comes into contact with the surrounding shallow trench isolation (STI) of the transistor. This effect could mitigate blooming issues but results in an increase of the pixel dark current. In this case, the interface states located in the STI act as generation centers inside the depleted volume of the photodiode, increasing the per-pixel dark current.

For the purpose of comparison two other PPD CIS devices were investigated in this study. These are also manufactured using a commercial CIS process from two other foundries. The MV imager has a depleted volume of around 10 $\mu\mathrm{m}^3$ and the SP imager around 1 $\mu\mathrm{m}^3$. The architectures are similar to the device under investigation, that is to say, 4T pixel CIS using PPD.

The external quantum efficiency, the charge-to-volt conversion factor and the dark current measurement were taken at 23°C. Activation energy of the dark current was determined by applying a wide temperature range from -10°C to 60°C as in [17]. The dark current random telegraph signal (DC-RTS) was detected using an automated detection method. This method is detailed in [13] and relies on a conventional edge detection technique. The measured temporal dark current of one pixel is filtered by a digital edge detection filter. When a pixel exhibiting dark current fluctuations is detected, the algorithm determines the number and the values of the discrete dark current levels, the maximum transition amplitude and the number of transitions during the observation. The entire pixel array is scanned to obtain the RTS characteristics of each individual pixel. The RTS measurement lasts for 10 hours, and dark current values are recorded every 2 seconds for all tests.

TABLE I
IRRADIATION CHARACTERISTICS

Imagers	Particles	Energy (MeV)	Fluence (cm^{-2})	DDD (TeV/g)	TID ($Gy(SiO_2)$)
IC 1	Proton	120	5×10^{9}	12	4
IC 2	Proton	120	2×10^{10}	48	16
IC 3	Neutron	14	5×10^{10}	183	<1
IC 4	Neutron	14	1×10^{12}	3650	<1
IC 5	Neutron	0.8	5×10^{14}	1.2×10^{6}	<1
MV 1	Proton	50	1.4×10^{10}	54	22
MV 2	Proton	50	5×10^{10}	194	79
SP	Proton	60	1×10^{11}	330	137

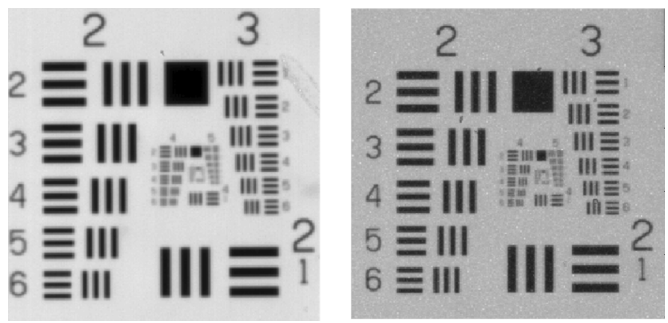

Fig. 3. Raw images of the 1951 USAF resolution test chart captured before irradiation (left) and after 1.2×10^6 TeV/g using 0.8 MeV neutrons (right).

Table I illustrates the irradiation performed on each tested imager. The sensors were exposed to neutron beams at CEA DAM Valduc and proton irradiation tests were performed at Kernfysisch Versneller Instituut (KVI) and at the Université Catholique de Louvain (UCL) facilities. All irradiations were performed at room temperature and all measurements were carried out three weeks after irradiations (Room temperature storage).

III. IMPACT ON THE ELECTRO-OPTIC PERFORMANCES

This section sets out the electro-optic performances after proton and neutron irradiations. As few publications report the impact on image quality, external quantum efficiency [8] or charge-to-volt conversion factor of only displacement damage in CIS, we therefore measured these parameters for each IC imager. Changes were solely observed for the IC5 device where the DDD reached 1.2×10^6 TeV/g. It is important to point out that for all other devices tested, the pre and post irradiation electro-optical parameters were the same.

Fig. 3 illustrates a raw image of the 1951 USAF resolution test chart using the IC5 PPD CIS. Even after 1.2×10^6 TeV/g using 0.8 MeV neutrons, we obtain a well resolved image of the test chart.

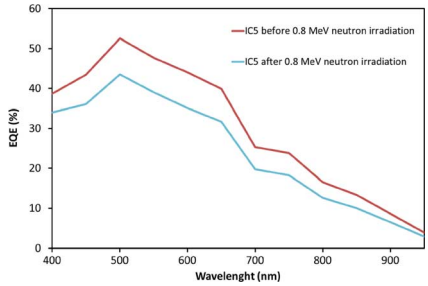

Fig. 4. External quantum efficiency before and after 1.2×10^6 TeV/g deposited dose using 0.8 MeV neutrons.

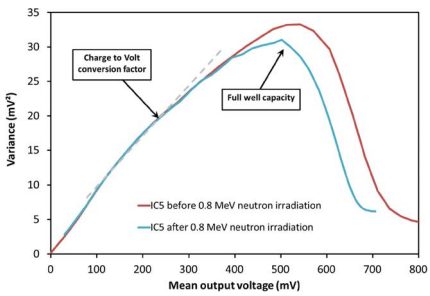

Fig. 5. Mean-variance curves before and after 1.2×10^6 TeV/g deposited dose using 0.8 MeV neutrons.

A. External Quantum Efficiency

The external quantum efficiency (EQE) measurement [14] is given in Fig. 4. After 0.8 MeV neutron irradiations, EQE drops for the whole visible wavelength range. The worst case appears for wavelength under 650 nm. This phenomenon could be due to a transmission coefficient change of the imager top layer or a change of the photodiode collection [15].

B. Charge-to-Volt Conversion Factor

Fig. 5 shows the mean-variance curve for the imager IC5 before and after the highest dose. The slope of the curve represents the charge-to-volt conversion factor (CVF) [16] and the peak of the curve gives the full well capacity (FWC) of the imager. As illustrated in the figure, the CVF is unchanged whereas the FWC decreases slightly. This last drop corresponds to a PPD modification, which will be covered in more detail in the next section.

IV. Impact on Dark Current

A. Mean Dark Current Increase

The mean dark current increase is investigated after proton and neutron exposures. The displacement damage dose deposited ranges from 12 TeV/g to 1.2×10^6 TeV/g. These results in PPD CIS are compared with previous results on 3T CIS. Fig. 6 presents the generation rate increase of PPD CIS with DDD. The results concerning PPD CIS are compared with previous 3T pixels CIS data from [17] and correlate with the universal damage factor (UDF) [18] estimation of the dark current increase. Fig. 6 shows a generally linear relationship between UDF and DDD. Such a relationship arises when displacement defect in the space charge region act as classical Shockley-Read-Hall (SRH) generators. Contrary to previous

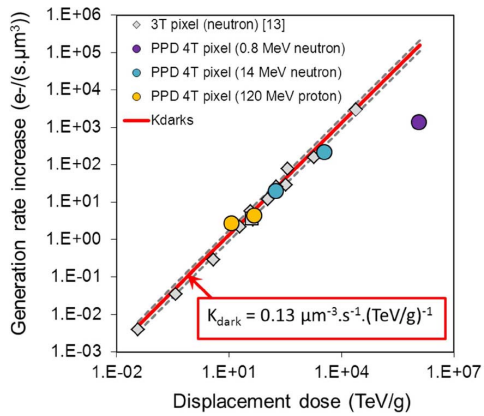

Fig. 6. Mean generation rate increase related to the mean dark current. Proton and neutron irradiation results agree with displacement contribution estimated using UDF. All devices are IC another 3T CIS from [17] is added to emphasize the correlation.

3T CIS studied [10], proton irradiation results for PPD CIS correlate with UDF. It could be explain by the fact that the space charge region of the PPD is not contacting the isolation oxide and therefore is almost independent of the TID-induced dark current [4]. This result is of great importance, proving as it does the significant impact of the displacement damage-induced dark current increase in PPD CIS irradiated with protons (in the energy and fluence range investigated). Concerning the highest DDD, the value is two orders of magnitude under the $\mathrm{K_{dark}}$ contribution. This phenomenon is due to the modification of the PPD. For the fluence above 10^{14} n.cm^2 the doping level could be modified $(\mathrm{N_{eff}})$ [19] inducing a reduction of the depleted volume size in all geometrical directions. For the IC5 imager, according to a cross section of 4.66 barns (for 0.8 MeV neutron using the GEANT 4 calculation code), the mean number of interactions per depleted microvolume is above 470. According to this phenomenon, we can consider that the depleted volume of the PPD could be reduced. This hypothesis could explain the EQE drop for all wavelengths and the reduction in FWC.

B. Dark Current Distribution Non-Uniformity

The dark current distributions after irradiations are presented in Fig. 7. Hot pixel tails behaving exponentially for each IC devices were observed in the semi-logarithmic scale. This behavior is also observed in 3T pixel after proton and neutron irradiations [5], [10]. However, as shown in Fig. 8, we noted an important change when performing a zoom at the beginning of the distribution curve. In proton irradiation, a peak appears in the exponential tail around 40 e^-/s. This phenomenon is also observed in the distribution of dark current increase of the imagers SP and MV, respectively represented in Figs. 9 and 10. This peak seems to be characteristic of proton irradiations because it is not clearly observed after neutron irradiations (Fig. 8). This phenomenon may be due to displacement damage and we attempt to clarify this issue in future work.

Such peaks are also reported in CCD [9], [20], [21] and mainly observed after metallic contamination. In these devices, the dark current level is extremely low and comes from the

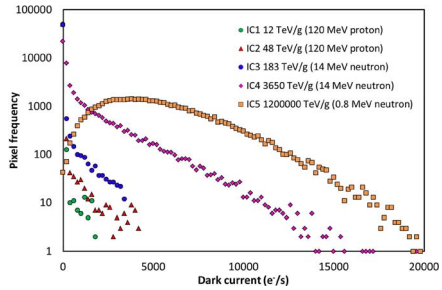

Fig. 7. Dark current distribution after irradiation for each IC imager tested. A common exponential behavior appears on the distributions.

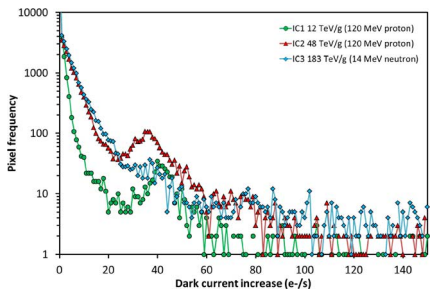

Fig. 8. Zoom on the first part of the dark current increase distribution. A specific peak appear for proton irradiation around 40 e^-/s whereas is not clearly observed for neutron irradiation.

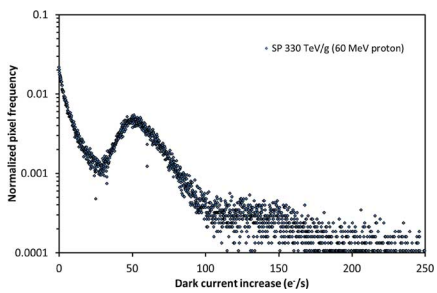

Fig. 9. Dark current increase distribution after 330 TeV/g deposited dose using 60 MeV proton. A peak around 50 e^-/s also appears in the distribution of the SP imager.

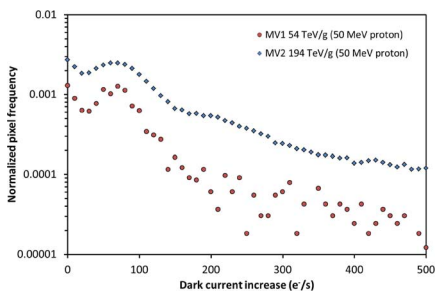

Fig. 10. Dark current increase distribution after 54 TeV/g and 194 TeV/g deposited dose using 50 MeV proton. A peak around 50 e^-/s also appears in the distributions of the MV imagers.

diffusion current, that is to say, there is no generation center located inside the depleted volume of the photosensitive element. Thus, when metallic contamination or defects due to irradiation occur in the depleted volume, the generation current appears and a peak appears in accordance with the generation rate of the defect. Therefore, the peaks correspond to a population of pixels containing the same small number of defects. For this

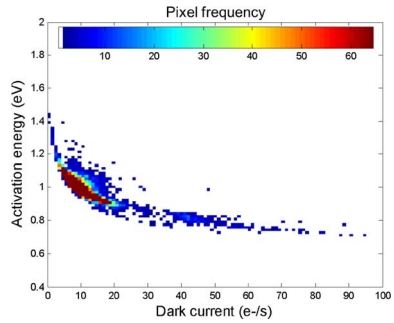

Fig. 11. Activation energy of the dark current plotted against dark current at 23°C. The dark current is induced by 120 MeV proton at 48 TeV/g deposited dose.

reason several peaks could appear for N times the same defect or for a defect with a different generation rate. The peaks are well-resolved for the metallic defects because the concentration of this defect is very low and it generation rate is high (energy level approaching the silicon mid-gap).

The authors [9], [20], [21] develop a method, called dark current spectroscopy, to characterized the nature of the defect responsible for dark current. This method can be applied using PPD CIS but must be used with caution to determine the nature of irradiation induced defects. This method could provide the generation rate of defects created after irradiation, meaning that the nature of the defect could be deduced. However, proton and neutron irradiations create several types of defect (point defects or clusters) with different generation rates. Therefore, it is possible to observe peaks at the beginning of the dark current increase distribution, but for a higher current, the pixels contain a large number of defects and these defects present different generation rates. Thus the peaks disappear giving way to what appears to be an exponential tail, generally referred to as a hot pixel tail in irradiated solid state imagers.

Particular care has to be taken when studying PPD CIS using more than 4 transistors inside the pixel. Indeed, adding another transistor for anti-blooming could introduce other sources of dark current, because the gates of these other transistors are not accumulated during integration. This other source could induce a higher dark current (one order of magnitude higher) and leads to the disappearance of the dark current peak at the beginning of the distribution.

C. Dark Current Spectroscopy and Activation Energy

To investigate the behavior of the dark current increase, the activation energy of the dark current was measured. Fig. 11 shows the dark current activation energy of each pixel on device IC 2. The energy is plotted against the dark current at 23°C and the coloring corresponds to pixel frequency at the same activation energy. The main part of the pixel is around 10 e^-/s and is unchanged after irradiation. Its activation energy is around 1.12 eV which implies a diffusion current mechanism, that is to say, the main contribution of the dark current comes from defects outside the space charge region. Therefore, the dark current in a pinned photodiode is mainly diffusion current before irradiation (using optimized Vlow TG). However, for pixels located in the hot pixel tail, the activation energy decreases and

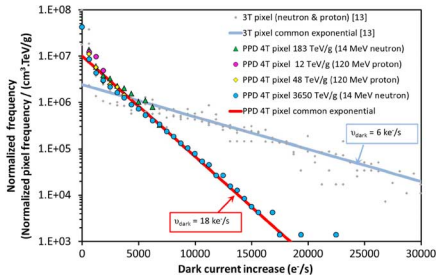

Fig. 12. Normalized histogram of the dark current increase for PPD CIS. Common exponential behavior is observed.

reaches almost mid-gap value for the highest dark current. Displacement damage induced electro-active defects located in the space charge region. These defects act as generation centers and contribute to the dark current which becomes a generation current (activation energy between 0.56 eV and 1.12 eV). Concerning the peak around 40 e^-/s, the activation energy is found to be around 0.8 eV. Under the hypothesis of the dark current spectroscopy, we consider that this peak corresponds to a pixel containing one defect. Moreover, under the assumption of UDF and following the conclusion about dark current increase origin in [19] we consider that this defect could be an intrinsic silicon defect.

Regarding the energy level of intrinsic defects [19] we suggest di-vacancy, V_2 $(-/0)$. Using the SRH equation and dark current spectroscopy [9], [20], [21], we obtain σ_p, the hole capture cross section, to be around 1.5×10^{-13} cm^2 and using the space charge region volume estimated with TCAD simulation, we suggest a probable concentration of around 2.5×10^{-11} $at.cm^{-3}$.

D. Modeling the Experimental Data

As for 3T pixel CIS, the dark current increase distribution in irradiated PPD CIS seems to behave exponentially. In previous studies [17], we attempt to model the dark current increase distribution using two factors, υ_{dark} and γ_{dark}, which seems to be common for 3T pixel CIS. The υ_{dark} is obtained when we normalized the distribution by number of pixels, the DDD and the depleted volume.

Fig. 12 illustrates this analysis. We observed behavior common to neutron and proton-induced dark current in PPD CIS. However, the common exponential parameter is around 18 ke^-/s in PPD CIS compared with 6 ke^-/s in 3T pixel CIS [17]. We note that results from IC 3 (PPD 4T pixel 183 TeV/g using 14 MeV neutron) are also given in a previous study [17] but was considered following the 6 ke^-/s exponential behavior due to the lack of point compare to other curves. Using this new set of PPD CIS data, we have clearly observed this different behavior which provides υ_{dark} around 18 ke^-/s.

The disagreement between 3T pixel CIS and PPD CIS could be explained by the small size of the depleted volume of the PPD. The PPD depleted volume is 50 times smaller than the smallest depleted volume investigated in 3T pixel CIS in [17].

As regard this discrepancy between PPD and 3T pixel CIS, we state that the model develop in [17] should be adapted and verify to be use with PPD CIS data.

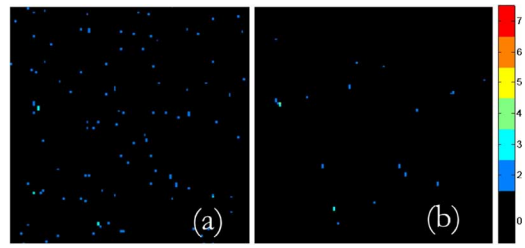

Fig. 13. Mapping of the detected DC-RTS using Vlow $TG = 0$ V (a) and Vlow $TG = -0.5$ V (b).

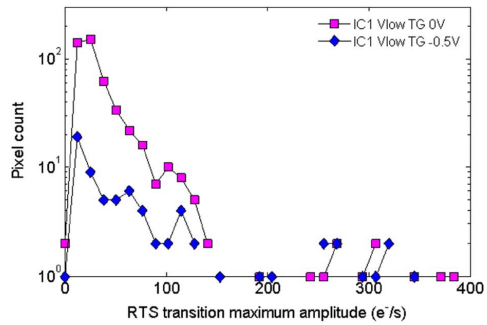

Fig. 14. Transition maximum amplitude distributions using Vlow $TG = 0$ V (Purple square) and Vlow $TG = -0.5$ V (blue diamond).

E. Dark Current Random Telegraph Signal

The DC-RTS [5], [22]–[24] was investigated in the PPD CIS. For this analysis we performed two different measurements. The first one using V_{Low} $TG = 0$ V during the integration time and the second one with V_{Low} $TG = -0.5$ V.

Fig. 13 shows the mapping of the 256 ×256 pixel array for both experiments (both Vlow TG) after proton irradiation (12 TeV/g). Colored pixels correspond to the pixel detected as RTS pixel and the color defines the number of level of the RTS.

The results show fewer DC-RTS pixels when the transfer gate is accumulated during the integration time. In addition, the maximum transition amplitude, which is a key parameter for DC-RTS [24], is also plotted for both experiments in Fig. 14. Using V_{Low} $TG = 0$ V during the integration time, the space charge region is extended under the transfer gate and touches the STI. TID induced DC-RTS is known to occur in trench oxide, due to meta-stable interface states [24]. Therefore, the main contribution to DC-RTS is certainly due to TID-induced DC-RTS using V_{Low} $TG = 0$ V. On the contrary, using V_{Low} $TG = -0.5$ V, the number of DC-RTS pixels falls and the histogram of the maximum transition amplitude is reduced. This effect suggests DDD induced DC-RTS [24]. It implies that the residual DC-RTS observed in Fig. 13(b), is due to a bulk meta-stable center. Therefore, when the PPD CIS is correctly operated to reduce dark current (Vlow $TG = -0.5$ V), we are able to eliminate TID-induced DC-RTS. This highlight the advantages of PPD CIS compared to 3T pixel CIS devices.

Fig. 15 illustrates IC 1, 2 and 3 using Vlow $TG = -0.5$ V. The increase of DC-RTS that we observed is therefore due to displacement damage. The common exponential behavior of DDD-induced DC-RTS found in 3T pixel CIS [24] is also plotted in this figure and the data for IC3 concords well with the common factor, λ_{DDD}. This suggests that the characteristic of defect related to DDD induced DC-RTS is the same in 4T

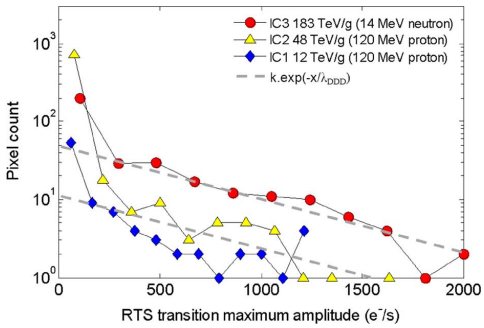

Fig. 15. Transition maximum amplitude distributions after 14 MeV neutron and 120 MeV proton irradiations. An exponential fit using λ_{DDD} is plotted.

pixel CIS than in 3T pixel CIS. Concerning IC 1 and 2, the comparison is difficult because the number of DC-RTS pixel is not enough in the histogram and the shape of the distribution is not correctly defined, making difficult any conclusion.

V. Conclusion

This is the first dedicated study on displacement damage effects in PPD CIS. Up to 3650 TeV/g, electro-optic performances (EQE, CVF, FWC) is unchanged. However, following an exposure to a DDD of 1.2×10^6 TeV/g (0.8 MeV neutron) these parameters degrade, reduction of EQE and FWC, probably due to a change in the PPD doping level.

As in 3T pixel CIS, the PPD CIS mean dark current increase with DDD and could be estimated using the universal damage factor. This implies that displacement damages induced defects in space charge region of the PPD and these defects lead to a classical SHR generation mechanism. This also implies that the DDD-induced dark current increase is proportional to the depleted volume of the 3T and 4T pixel CIS. After proton and neutron irradiation, a common hot pixel tail appears on the dark current distribution and behaves exponentially. Moreover, PPD CIS have proven to be excellent devices to study displacement damage-induced dark current increase in silicon. Firstly, as with other solid state imagers, the large amounts of pixels in the array provide an interesting statistic and the phenomenon is sampled according to the microvolume used (around 4 μm^3). But, as PPD CIS are very high-performance in terms of dark current levels, they make it possible to investigate the electro-activity of displacement damage-induced defects. Using the dark current spectroscopy, we identified the defect type and energy created by displacement damage.

Finally, we report DDD-induced DC-RTS in pinned photodiode. We found that the maximum transition amplitude is a useful tool for studying DC-RTS.

Acknowledgment

The authors would like to thank the CIMI group for their help, especially P. Martin-Gonthier for the sensor conception, P. Cervantes, M. Estribeau and B. Avon for their help in measurements, S. Rolando and R. Molina for their critical point of view about the study. They would also thank S. Quenard, Y. Leo, CEA, Valduc, M. Boutillier, CNES and G. Berger, UCL, Belgium, for their assistance during neutron and proton irradiations.

References

[1] P. Lee, R. Gee, M. Guidash, T. Lee, and E. R. Fossum, "An active pixel sensor fabricated using CMOS/CCD process technology," in *Proc. IEEE Workshop CCDs Adv. Image Sens.*, 1995, pp. 115–119.

[2] P. R. Rao, X. Wang, and A. J. P. Theuwissen, "Degradation of CMOS image sensors in deep-submicron technology due to γ -irradiation," *Solid-State Electron.*, vol. 52, no. 9, pp. 1407–1413, Sep. 2008.

[3] M. Innocent, "A radiation tolerant 4t pixel for space applications," in *Proc. IISW*, 2009.

[4] V. Goiffon, C. Virmontois, P. Magnan, P. Cervantes, M. Gaillardin, S. Girard, P. Paillet, and P. Martin-Gonthier, "Identification of radiation induced dark current sources in pinned photodiode CMOS image sensors," in *Proc. RADECS*, 2011.

[5] G. R. Hopkinson, "Radiation effects in a CMOS active pixel sensor," *IEEE Trans. Nucl. Sci.*, vol. 47, no. 6, pp. 2480–2484, Dec. 2000.

[6] J. Bogaerts, B. Dierickx, and G. Meynants, "Enhanced dark current generation in proton-irradiated CMOS active pixel sensors," *IEEE Trans. Nucl. Sci.*, vol. 49, no. 3, pp. 1513–1521, Jun. 2002.

[7] M. Beaumel, D. Herve, and D. Van Aken, "Cobalt-60, proton and electron irradiation of a radiation-hardened active pixel sensor," *IEEE Trans. Nucl. Sci.*, vol. 57, no. 4, pp. 2056–2065, Aug. 2010.

[8] M. Deveaux, G. Claus, G. Deptuch, W. Dulinski, Y. Gornushkin, and M. Winter, "Neutron radiation hardness of monolithic active pixel sensors for charged particle tracking," *Nucl. Instr. Meth. A*, vol. 512, pp. 71–76, 2003.

[9] R. D. McGrath, J. Doty, G. Lupino, G. Ricker, and J. Vallerga, "Counting of deep-level traps using a charge-coupled device," *IEEE Trans. Electron Devices*, vol. ED-34, no. 12, pp. 2555–2557, Dec. 1987.

[10] C. Virmontois, V. Goiffon, P. Magnan, S. Girard, C. Inguimbert, S. Petit, G. Rolland, and O. Saint-Pe, "Displacement damage effects due to neutron and proton irradiations on CMOS image sensors manufactured in deep sub-micron technology," *IEEE Trans. Nucl. Sci.*, vol. 57, no. 6, pp. 3101–3108, Dec. 2010.

[11] A. J. P. Theuwissen, "CMOS image sensors: State-of-the-art," *Solid-State Electron*, vol. 52, no. 9, pp. 1401–1406, Sep. 2008.

[12] T. Watanabe, J.-H. Park, S. Aoyama, K. Isobe, and S. Kawahito, "Effects of negative-bias operation and optical stress on dark current in CMOS image sensors," *IEEE Trans. Electron Devices*, vol. 57, no. 7, pp. 1512–1518, Jul. 2010.

[13] V. Goiffon, P. Magnan, O. Saint-Pé, F. Bernard, and G. Rolland, "Multi level RTS in proton irradiated CMOS image sensors manufactured in a deep submicron technology," *IEEE Trans. Nucl. Sci.*, vol. 56, no. 4, pp. 2132–2141, Aug. 2009.

[14] A. El Gamal and H. Eltoukhy, "CMOS image sensors," *IEEE Circuits Devices Mag.*, vol. 21, no. 3, pp. 6–20, May 2005.

[15] P. R. Rao, X. Wang, and A. J. P. Theuwissen, "Degradation of CMOS image sensors in deep-submicron technology due to -irradiation," *Solid-State Electron.*, vol. 52, no. 9, pp. 1407–1413, Sep. 2008.

[16] B. Pain and B. Hancock, "Accurate estimation of conversion gain and quantum efficiency in CMOS imagers," in *Proc. SPIE*, 2003, vol. 5017, p. 94.

[17] C. Virmontois and V. Goiffon, "Similarities between proton and neutron induced dark current distribution in CMOS image sensors," *IEEE Trans. Nucl. Sci.*, vol. 59, no. 4, pp. 927–937, Aug. 2012.

[18] J. R. Srour and D. H. Lo, "Universal damage factor for radiation-induced dark current in silicon devices," *IEEE Trans. Nucl. Sci.*, vol. 47, no. 6, pp. 2451–2459, Dec. 2000.

[19] M. Moll, "Radiation Damage in Silicon Particle Detectors," Ph.D. dissertation, Universität Hamburg, Hamburg, 1999.

[20] W. C. McColgin, J. P. Lavine, J. Kyan, D. N. Nichols, and C. V. Stancampiano, "Dark current quantization in CCD image sensors," in *IEDM Tech. Dig.*, 1992.

[21] C. Tivarus and W. C. McColgin, "Dark current spectroscopy of irradiated CCD image sensors," *IEEE Trans. Nucl. Sci, vol*, vol. 55, no. 3, pp. 1719–1724, Jun., 2008.

[22] J. Bogaerts, B. Dierickx, and R. Mertens, "Random telegraph signals in a radiation-hardened CMOS active pixel sensor," *IEEE Trans. Nucl. Sci.*, vol. 49, no. 1, pp. 249–257, Feb. 2002.

[23] V. Goiffon, P. Magnan, P. Martin-Gonthier, C. Virmontois, and M. Gaillardin, "Evidence of a novel source of random telegraph signal in CMOS image sensors," *IEEE Electron Device Lett.*, 2011, submitted for publication.

[24] C. Virmontois, V. Goiffon, P. Magnan, S. Girard, S. Petit, G. Rolland, and O. Saint-Pé, "Total ionizing dose versus displacement damage dose induced dark current random telegraph signals in CMOS image sensors," *IEEE Trans. Nucl. Sci.*, vol. 58, no. 6, Dec. 2011.